Beyond the Axoneme: Whole-Cell Proteomics Identifies Novel Regulators of Ciliogenesis in *Xenopus* Epidermal Multiciliated Cells

Xiaolu Xu[1], Yanbao Yu[2], Tony Zheng[1], Fiona Clark[1], Jean Ross[3], Andre L P Tavares[1], Shuo Wei[1,*], Jian Sun[1,4,*]

[1] Department of Biological Sciences, University of Delaware, Newark, DE 19716, USA
[2] Department of Chemistry and Biochemistry, University of Delaware, Newark, DE, 19716, USA.
[3] BioImaging Center, Delaware Biotechnology Institute, Newark, DE, 19713, USA
[4] Lead contact
*Correspondence: swei@udel.edu; jiansun@udel.edu

SUMMARY

Motile cilia generate directional fluid flow critical for development and tissue homeostasis, and their dysfunction underlies a range of human diseases. Prior proteomic studies have focused on isolated axonemes, leaving the regulatory components located in other cellular compartments of multiciliated cells (MCCs) largely unidentified. To bridge this gap, we performed whole-cell proteomic profiling of multicilin-induced *Xenopus* animal cap-derived mucociliary organoids, which are highly enriched in MCCs. Leveraging On-Filter In-Cell (OFIC) processing and mass spectrometry, we identified over 9,000 proteins, including 832 upregulated in MCCs. These encompassed both established ciliary components and novel candidates localized to distinct ciliary structures. Functional validation confirmed the involvement of previously uncharacterized proteins in cilium formation and MCC differentiation. This study presents a high-resolution, whole-cell proteome of vertebrate MCCs, providing critical insights into the molecular networks that govern ciliogenesis and offering a valuable resource for understanding the mechanisms of cilia-related disorders.

KEYWORDS

Motile cilia, multiciliated cells, ciliogenesis, proteomics, whole-cell, axoneme, On-Filter In-Cell

INTRODUCTION

Motile cilia are microtubule-based organelles that generate directional fluid flow, playing fundamental roles in biological processes such as mucus clearance in the respiratory tract, cerebrospinal fluid circulation, and embryonic development.[1-4] Dysfunction of motile cilia results in ciliopathies, a group of disorders associated with chronic respiratory infections, hydrocephalus, and infertility.[5,6] Despite significant progess in understanding ciliary structure and function, many molecular regulators of ciliogenesis remain unidentified.

Proteomic approaches have been instrumental in mapping the molecular composition of cilia, leading to the identification of numerous proteins involved in cilia assembly and function.[7] Early proteomic analyses of ciliary axonemes from human bronchial epithelial cells identified over 200 proteins, including core ciliary components such as tubulins and dyneins.[8] Subsequent mass spectrometry (MS)-based studies expanded the ciliary proteome, identifying 352 axonemal proteins, including multiple tubulin isoforms and various non-tubulin constituents.[9] In *Xenopus laevis*, proteomic characterization of isolated cilia has identified thousands of ciliary proteins, including keratin 17, which plays a crucial role in ciliogenesis.[10]

Comparative studies in *Chlamydomonas reinhardtii* and *Trypanosoma* have further revealed evolutionarily conserved ciliary proteins, identifying homologs of vertebrate disease-related proteins such as polycystin 2, fibrocystin, and hydin.[11-14]

Although these studies have significantly advanced our understanding of ciliary protein composition, they primarily relied on purified cilia isolated from cultured cells, *Xenopus* embryos, *Chlamydomonas*, or *Trypanosomes* using chemical or mechanical treatments to enrich for ciliary protein.[8-14] While these approaches have provided valuable insights into the axonemal proteome, they focus exclusively on the ciliary axoneme while overlooking other critical cellular components involved in ciliogenesis. MCC function is regulated not only by axonemal proteins but also by basal bodies, cytoplasmic factors, and nuclear components.[2,3] The reliance on deciliation, axoneme isolation, or shedding in previous studies has largely overlooked these regulatory elements. To address this limitation, a more comprehensive proteomic approach is desired to capture the entire molecular network governing cilia formation and function. Thus, expanding proteomic profiling to whole epidermal MCCs is essential for providing a broader perspective on ciliogenesis by incorporating proteins from all cellular compartments involved in MCC development.

The embryonic epidermis of *Xenopus* has emerged as a powerful vertebrate model for studying normal ciliogenesis and ciliopathies as its cellular composition, which includes both multiciliated and secretory cells, closely resembling the mammalian airway epithelium.[15,16] Many key proteins involved in mucociliary differentiation and function are conserved between *Xenopus* and mammals.[17,18] Additionally, *Xenopus* animal caps, pluripotent cell sheets derived from the animal pole of blastula-stage embryos, serve as an effective *ex vivo* model. When cultured as explants, these organoids undergo default mucociliary differentiation, faithfully recapitulating early developmental events and providing a tractable system for investigating MCC biology.[15,19]

We recently developed On-Filter In-Cell (OFIC)-based sample preparation as a robust strategy for high-sensitivity proteomic analysis, reducing processing variability and enabling efficient detection of low-abundance proteins, particularly in complex biological samples.[20,21] Unlike conventional lysis-based approaches, which require multiple processing steps that may introduce sample loss and biases, OFIC preserves the spatial organization of proteins while maintaining biochemical integrity. This method drastically streamlines proteomic workflows, making it particularly advantageous for low sample inputs and enabling more comprehensive investigations of MCCs at a systems level.

By leveraging *Xenopus* animal cap–derived mucociliary organoids in combination with OFIC sample processing and mass spectrometry, we generated a high-resolution, cell type–enriched proteomic profile of whole MCCs. In particular, ectopic expression of multicilin (MCI), a master regulator of centriole assembly and ciliogenesis,[22,23] robustly induces MCC cell fate in animal caps and enriches ciliary proteins, thereby eliminating the need for axoneme isolation and expanding the detection of ciliary proteins to whole cells. Functional validation through *in situ* hybridization, immunostaining, and gene knockdown revealed several previously uncharacterized proteins that are essential for MCC formation and ciliogenesis. This comprehensive characterization of the MCC proteome provides valuable insights into the molecular networks driving ciliogenesis. Our findings not only broaden the catalogs of known ciliary proteins but also identify novel regulatory factors, offering new perspectives for understanding cilia-related diseases and advancing potential therapeutic approaches.
.

RESULTS

Generation of a Comprehensive MCC Proteome Using Animal Cap Organoids Induced with MCI-GR for MCC Enrichment

To generate a comprehensive and MCC-specific proteomic profile, we employed Xenopus laevis animal cap organoids as an ex vivo system to model MCC differentiation (Figure 1A). A major obstacle in whole-cell proteomic studies of MCCs is the challenge of distinguishing MCC-specific proteins from the other cellular proteins that can obscure the identification of bona fide regulators of ciliogenesis. To overcome this obstacle, we used the MCI fused with glucocorticoid receptor (GR) to selectively enhance MCC differentiation, based on prior studies showing that MCI promotes centriole biogenesis and ciliogenesis in both *Xenopus* epidermis and mammalian airway epithelial cells.[22,23] This strategy created an inducible MCC gain-of-function model, in which dexamethasone (Dex) treatment robustly induced MCC formation within the organoids. By comparing the proteomic profiles of Dex-treated and untreated animal cap organoids, we were able to enrich for proteins upregulated in MCCs, thereby reducing the background noise and enhancing the specificity of the proteomic dataset. To achieve temporal control and minimize early developmental toxicity, MCI-GR was overexpressed at one-cell stage, followed by dissection of animal caps at blastula stages (stage 8-9). Explants were cultured until stage 11, when Dex was added to activate MCI-GR, resulting in robust MCC differentiation by stage 26. Compared to untreated controls, Dex-treated organoids exhibited a marked increase in MCC formation, as confirmed by acetylated-tubulin staining (Figure 1B).

High-Depth Proteomic Profiling of MCCs Using OFIC Processing and LC-MS

Given the small size of animal cap organoids (diameter <0.5 mm), conventional lysis-based proteomic workflows require a large number of samples and multiple processing steps, potentially leading to inefficiencies and protein loss. To overcome these limitations, OFIC processing was used, enabling direct protein digestion in fixed cells while minimizing sample loss and enhancing proteomic depth.[20,21] Unlike conventional methods, which require nearly 100 organoids per replicate, the OFIC-based approach enabled robust proteomic analysis using only eight organoids per replicate across three biological replicates (Figure 1A).

LC-MS analysis identified over 9000 proteins, indicating high proteome coverage. The Pearson correlation averaged from 0.97 to 0.98 within biological replicates (Figure 1C), confirming high reproducibility of the OFIC method. Principal Component Analysis (PCA) showed distinct separation of Dex+ from Dex− groups (Figure 1D), highlighting substantial proteomic differences between MCC-enriched and control conditions. Comparative analysis identified 832 upregulated proteins in Dex+ MCCs, including well-known ciliary components such as Ccp110, Cep164, Rsph1, Dnai1, and Dnaaf4 (Figure 1E).[24-28]

Gene Ontology (GO) analysis revealed significant enrichment of cilia-associated proteins, including components of both basal bodies and axonemes (Figure 1F). In contrast to previous *Xenopus* proteomic studies that focused on isolated axonemes and excluded basal body proteins,[10] our whole-cell proteomics captured a more complete ciliary protein landscape. To further assess dataset quality, we compared the identified proteins to two established ciliary gene databases: MCC Core Genes and SYSCILIA.[29,30] We

found 298 and 186 overlapping proteins, respectively (Figure 1G and 1H). The significant overlap validates the biological relevance of our dataset and suggests the discovery of novel ciliary regulators, further emphasizing the advantage of our whole-cell approach over axoneme-focused studies.

Localization of Novel Ciliary Candidate Proteins to Diverse Ciliary Structures

To validate the novel candidates, four uncharacterized proteins—Coiled-Coil Domain-Containing 30 (Ccdc30), Membrane Occupation and Recognition Nexus-motif protein 2 (Morn2), Migration and Invasion Inhibitory Protein (Miip) and WD Repeat Domain 88 (Wdr88) were selected. Whole-mount *in situ* hybridization confirmed that all four genes were specifically expressed in epidermal MCCs, with *miip* showing earlier expression at stages 17-18, just before MCC ciliation (Figure 2A).

Subcellular localization was assessed by overexpressing GFP-tagged versions of each candidate in MCCs. Ccdc30 was detected as a ring-like structure surrounding the centrioles, resembling basal body appendages (Figure 2B). Morn2, predicted to function in the dynamic regulation of acrosome biogenesis during late spermiogenesis,[31] was detected along the axoneme but not at basal bodies (Figure 2C). Miip, which was initially identified as a binding partner of insulin-like growth factor-binding protein 2 (IGFBP2) and may function as an inhibitor of cell migration and invasion,[32] was localized exclusively to basal bodies (Figure 2D). Wdr88 was also associated with basal bodies but displayed an expanded appendage-like pattern overlapping with Centrin4-RFP (Figure 2E).

Morn2 and Ccdc30 are Novel Regulators of Ciliogenesis

To investigate the roles of candidate ciliary proteins, we selected Morn2 and Ccdc30, and carried out loss of function experiments. First, embryo gliding assays were conducted to evaluate ciliary function, as coordinated MCC ciliary beating drives embryo movement. Knockdown of Morn2 by a translation-blocking morpholino (MO) significantly impaired embryo gliding, which was rescued by co-injection of Morn2 MO-resistant mRNA (Figure 3A and 3B), indicating an essential role for this protein in MCC function. To determine whether gliding defects were due to deficient ciliogenesis, immunostaining for acetylated-tubulin was performed. Morn2 depletion resulted in a dramatic reduction in motile cilia, which was restored by Morn2 MO-resistant mRNA (Figure 3C and 3D), demonstrating that Morn2 is required for ciliogenesis of MCC. Scanning electron microscopy (SEM) further confirmed that Morn2 knockdown led to a significant reduction in cilia number and length (Figure 3E-3F). Despite the profound impact on cilia formation, further analysis indicated that Morn2 knockdown did not alter basal body number or their apical docking (Figure 3G-3I). This observation aligns with its subcellular localization restricted to the axoneme and supports a model in which Morn2 acts downstream of basal body positioning to promote axoneme assembly and ciliary elongation.

In the case of Ccdc30, knockdown of this protein by a specific MO also severely impaired embryo gliding (Figure 4A and 4B). Unlike Morn2 knockdown, Cilia staining showed that depletion of Ccdc30 not only impaired ciliogenesis but also decreased the overall number of MCCs (Figure 4C-4E), indicating its involvement in both ciliogenesis and MCC formation. Whole-mount *in situ* hybridization using the MCC specific marker foxj1, a transcriptional regulator of multiciliogenesis,[33] further confirmed that depletion of Ccdc30 inhibited epidermal MCCs formation, a phenotype that could be rescued by co-injection of Ccdc30 MO-resistant mRNA (Figure 4F and 4G). SEM analysis confirmed the reduction in cilia number without compromising cilia length, reinforcing the role of Ccdc30 in ciliogenesis (Figure 4H and 4I). Given that Ccdc30 is localized to a ring-like structure reminiscent of basal body appendages, we performed co-staining with the distal appendage marker protein Cep164.[28] Notably, Ccdc30 showed minimal overlap with Cep164 and appeared as a larger, more distally positioned ring structure as compared to Cep164

(Figure S1A; Video S1). Furthermore, Cep164 accumulation was preserved in the majority of centrioles in Ccdc30 morphants (Figure S1B), indicating that distal appendage formation and centriole maturation are likely unaffected by Ccdc30 depletion. However, a marked reduction in centriole number was observed in Ccdc30 morphants (Figure S1B; Figure 4J and 4K), a defect that was fully rescued by co-injection of morpholino-resistant Ccdc30 mRNA, indicating a critical role for Ccdc30 in centriole amplification. Beyond centriole biogenesis, ciliogenesis also relies on the formation of the apical actin meshwork and the proper migration and docking of basal bodies to the apical surface.[34-39] In Ccdc30-depleted MCCs, basal bodies failed to dock efficiently, accompanied by a significant loss of phalloidin staining, which reflects disruption of the apical actin network. Consequently, the apical surface area of MCCs was significantly reduced (Figure 4L and 4M). Collectively, these findings suggest that, in contrast to Morn2, which functions directly in axoneme assembly, Ccdc30 plays broader roles during MCC development. At earlier stages, Ccdc30 may contribute to MCC fate determination and centriole amplification; during ciliogenesis, it likely supports apical actin organization necessary for basal body migration and docking.

DISCUSSION

Motile cilia are essential for fluid propulsion in diverse biological contexts, and their dysfunction contributes to a wide spectrum of human diseases.[1-3] Despite extensive efforts to elucidate the molecular architecture of motile cilia, many regulators of ciliogenesis remain unknown, in part due to methodological limitations. Prior proteomic studies have predominantly focused on purified ciliary axonemes to enrich for ciliary proteins.[8-14] This approach, while informative, excludes key regulatory components located in other cellular compartments such as basal bodies, cytoplasm, and nuclei. Our study addresses this gap by presenting a high-resolution, whole-cell proteomic profile of vertebrate MCCs, generated using *Xenopus laevis* mucociliary organoids in combination with an MCI-driven enrichment strategy and OFIC-based proteomics.

The use of a glucocorticoid-inducible MCI expression system enabled robust MCC induction in animal cap organoids, creating a gain-of-function model that facilitated the enrichment of MCC-specific proteins. Comparing proteomes between Dex-treated and untreated samples allowed us to isolate proteins specifically associated with MCC identity and ciliogenesis. This strategy overcomes a key challenge in whole-cell proteomics—the presence of background signals from non-MCC cell types—and enhances the specificity of candidate identification. Through this approach, we identified over 9,000 proteins, with 832 significantly upregulated in MCCs, including well-established ciliary proteins such as Ccp110, Cep164, and Dnai1. GO enrichment and database comparisons validated the quality and relevance of our dataset and highlighted its utility in identifying novel regulators of motile cilia.

Beyond cataloging known ciliary components, this study uncovers several previously uncharacterized proteins with distinct subcellular localizations and functional relevance. For instance, we show here that Morn2 is localized along the axoneme and is essential for axoneme formation, acting downstream of basal body docking. In contrast, Ccdc30 was found to function at multiple levels of MCC development. It was required not only for centriole amplification but also for apical actin meshwork organization and basal body docking—processes that are essential for the formation of functional motile cilia. The localization of Ccdc30, which forms a larger ring-like structure distal to the known basal body appendage marker Cep164, suggests that it may define a novel subdomain of the basal body or associate with a distinct structural element involved in basal body maturation. One possibility is that Ccdc30 localizes to the base of the ciliary pocket, a region closely linked to actin organization. This could explain the disrupted apical actin meshwork observed in Ccdc30-depleted MCCs, consistent with the ciliary pocket's known role in coordinating actin dynamics and vesicle trafficking.[40] Notably, Ccdc30 has been recently reported in association with asthma exacerbation in patients.[41] While this association does not directly implicate

Ccdc30 in primary ciliary dyskinesia (PCD)-a genetic disorder caused by defects in motile cilia structure and function, asthma is a well-recognized comorbidity in children with PCD.[42] This clinical correlation further supports a functional link between Ccdc30 and motile cilia biology, raising the possibility that Ccdc30 plays a conserved role in the coordination of ciliary assembly and epithelial homeostasis relevant to human ciliopathies.

In conclusion, these findings demonstrate the power of whole-cell proteomics in combination with functional genomics to uncover new components and mechanisms of ciliogenesis. Importantly, the approach outlined here is generalizable and may be applied to other specialized cell types where proteome complexity and cell heterogeneity present analytical challenges. Furthermore, our data provide a rich resource for future studies of MCC development and cilia-related pathologies. This study not only expands the known repertoire of ciliary proteins but also sheds light on novel regulatory pathways in motile cilia formation and MCC differentiation. By moving beyond axoneme-centric methods, we reveal new layers of complexity in the assembly and function of motile cilia. These insights have broad implications for understanding the molecular basis of ciliopathies and for developing targeted therapeutic strategies to restore or enhance ciliary function in disease contexts.

RESOURCE AVAILABILITY

Lead contact

Further information and requests for reagents may be directed to and will be fulfilled by the Lead Contact, Jian Sun (jiansun@udel.edu).

ACKNOWLEDGMENTS

This work is supported by NIH R01 DE029802. Microscopy equipment was acquired with a shared instrumentation grant (S10 OD025165) and access was supported by NIH—NIGMS (P20 GM103446), NIGMS (P20 GM139760) and the State of Delaware. We also would like to acknowledge support from the National Institute of General Medical Sciences (NIGMS) under award number P20GM104316 for the Orbitrap Eclipse MS instrument. The MCI-GR construct was kindly provided by Brian Mitchell. The table of content figure and some of the main figures were created with BioRender.

AUTHOR CONTRIBUTIONS

J.S. conceived and designed the study. J.S. and X.X. performed the majority of the experiments, with assistance from T.Z. and F.C.. J.R. conducted scanning electron microscopy. Y.Y. carried out the LC-MS. A.L.P.T. provided *xenopus laevis* animals. J.S. drafted the manuscript. X.X. analyzed the data and prepared the figures. S.W. supervised the project and revised the manuscript. All authors contributed to data interpretation and approved the final version.

DECLARATION OF INTERESTS

The authors declare no competing interests.

SUPPLEMENTAL INFORMATION

Document S1 (this is the main PDF)

Video S1. Immunostaining of Ccdc30-HA and Cep164 in *X. tropicalis* epidermal MCC.
Centrin4-RFP (cyan), Cep164 (magenta), and Ccdc30-HA (green) are shown. The image, cropped from Figure S1A, highlights two basal bodies to visualize subcellular localization in greater detail. The video includes rotational views of the basal bodies to illustrate the spatial relationship between Ccdc30 and Cep164, a known distal appendage marker.

FIGURE TITLES AND LEGENDS

Figure 1. Profiling MCC proteome using *Xenopus* animal cap organoids with OFIC approach.
(A) Illustrative workflow of the proteomic analysis of *Xenopus* animal caps enriched with MCCs. Upon fertilization, embryos were injected with mRNA encoding MCI-hGR and then cultured to stage 9, when animal caps were dissected and cultured *in vitro* to generate organoids. With addition of dexamethasone, the majority of epidermal cells undergo differentiation toward a MCC fate, as compared to Dex-animal caps. The organoids were cultured to stage 26 and were fixed with methanol. E4tip was used for OFIC processing. The mass spectrometric analysis was performed using Orbitrap Eclipse.

(B) Organoids were fixed at stage 26 and stained for acetylated tubulin (Ac-tub). mRNA encoding a membrane-bound form of GFP (memGFP) was co-injected as a tracer to label targeted cells. Representative confocal images of the epidermis for each condition were shown.

(C) Pearson correlation analysis.

(D) Principal component analysis.

(E) Volcano plot of comparison between Dex-treated organoids and non-treated ones. Well-characterized ciliary proteins were labeled.

(F) Gene ontology cellular component analysis of significantly upregulated proteins in (E).

(G) Venn diagram showing the overlap between significantly upregulated proteins in (E) and the MCC core gene database. Note that protein counts from our dataset were adjusted by merging L and S isoforms of the same gene and excluding uncharacterized proteins. The p-value was calculated using a hypergeometric distribution test.

(H) Venn diagram showing the overlap between significantly upregulated proteins in (E) and Syscilia database. Note that protein counts were adjusted to reflect human orthologs mapped from our dataset. The p-value was calculated using a hypergeometric distribution test.

Figure 2. Expression and subcellular localization of candidate novel ciliary proteins in epidermal MCCs.
(A) Whole-mount *in situ* hybridization showing the expression of *ccdc30*, *morn2* and *wdr88* in epidermal MCCs at stage 22-24, followed by immunostaining with anti–acetylated tubulin to mark motile cilia. All three genes were specifically expressed in MCCs, with *miip* displaying earlier expression at stages 17–18, prior to ciliation.

(B–E) Live imaging of MCCs overexpressing GFP-tagged candidate proteins with Centrin4-RFP marking basal bodies. Ccdc30-GFP (B) formed a ring-like structure surrounding basal bodies, resembling basal body appendages. Morn2-GFP (C) localized along the axoneme but was absent from basal bodies. Miip-GFP (D) localized exclusively to basal bodies. Wdr88-GFP (E) was associated with basal bodies and exhibited an expanded appendage-like pattern overlapping with Centrin4-RFP. Scale bars: 10 µm.

Figure 3. Morn2 is essential for ciliogenesis of MCCs.
(A and B) Gliding assay showing that Morn2 knockdown significantly impaired embryo motility, a phenotype rescued by co-injection of Morn2 MO-resistant mRNA. Scale bars: 1000 µm. Quantification of

gliding velocity in (A) from three independent experiments with unpaired two-tailed t-tests. Mean ± s.d. values are presented. ns: no statistical differences between the groups.

(C and D) Immunostaining for acetylated tubulin reveals a dramatic loss of motile cilia in Morn2 morphants, which is rescued by Morn2 mRNA re-expression. Scale bars: 50 µm. Quantification of normalized intensity of acetylated-tubulin in (C) from three independent experiments with unpaired two-tailed t-tests. Mean ± s.d. values are presented.

(E and F) Scanning electron microscopy (SEM) of MCCs shows a marked reduction in cilia number and length upon Morn2 depletion, with restoration following rescue. Scale bars: 10 µm. Quantification of cilium length in (E) from three independent experiments with unpaired two-tailed t-tests. Mean ± s.d. values are presented.

(G-I) Phalloidin staining for actin network and Centrin4-RFP for basal bodies indicate that basal body number and apical docking remain largely unaffected in Morn2 morphants. Scale bars: 10 µm. Quantification of centriole number per MCC in (G) from three independent experiments with unpaired two-tailed t-tests. Mean ± s.d. values are presented. Quantification of apical surface area in (G) from three independent experiments with unpaired two-tailed t-tests. Mean ± s.d. values are presented. ns: no statistical differences between the groups.

Figure 4. Ccdc30 regulates MCC differentiation, centriole amplification, and apical cytoskeletal organization.

(A and B) Gliding assay showing that knockdown of Ccdc30 severely impaired embryo motility, which was rescued by co-injection of Ccdc30 MO-resistant mRNA. Scale bars: 1000 µm. Quantification of gliding velocity in (A) from three independent experiments with unpaired two-tailed t-tests. Mean ± s.d. values are presented.

(C-E) Immunostaining for acetylated tubulin demonstrates that Ccdc30 depletion reduces cilia number and blocks MCC formation. Scale bars: 50 µm. Quantification of normalized intensity of acetylated-tubulin in (C) from three independent experiments with unpaired two-tailed t-tests. Mean ± s.d. values are presented. Quantification of MCC number in (C) from three independent experiments with unpaired two-tailed t-tests. Mean ± s.d. values are presented.

(F and G) Whole-mount *in situ* hybridization using the MCC marker *foxj1* confirms that Ccdc30 knockdown inhibits MCC formation, a phenotype reversed by Ccdc30 mRNA rescue. Scale bars: 500 µm. Quantification of MCC number in (F) from three independent experiments with unpaired two-tailed t-tests. Mean ± s.d. values are presented.

(H and I) Scanning electron microscopy reveals a dramatic reduction in cilia number and length in Ccdc30 morphants. Scale bars: 10 µm. Quantification of cilium length in (H) from three independent experiments with unpaired two-tailed t-tests. Mean ± s.d. values are presented.

(J-M) Phalloidin staining (actin) and Centrin4 (basal bodies) show that in Ccdc30 morphants, centriole number is reduced, and basal body docking is impaired. Phalloidin signal at apical surface area is also significantly diminished. Scale bars: 10 µm. Quantification of centriole number in (J) from three independent experiments with unpaired two-tailed t-tests. Mean ± s.d. values are presented. Quantification of apical surface area in (J) from three independent experiments with unpaired two-tailed t-

tests. Mean ± s.d. values are presented. Quantification average phalloidin intensity in (J) from three independent experiments with unpaired two-tailed t-tests. Mean ± s.d. values are presented.

REFERENCES

1. Fliegauf, M., Benzing, T., and Omran, H. (2007). When cilia go bad: cilia defects and ciliopathies. Nat Rev Mol Cell Biol *8*, 880-893. 10.1038/nrm2278.
2. Brooks, E.R., and Wallingford, J.B. (2014). Multiciliated cells. Curr Biol *24*, R973-982. 10.1016/j.cub.2014.08.047.
3. Spassky, N., and Meunier, A. (2017). The development and functions of multiciliated epithelia. Nat Rev Mol Cell Biol *18*, 423-436. 10.1038/nrm.2017.21.
4. Boutin, C., and Kodjabachian, L. (2019). Biology of multiciliated cells. Curr Opin Genet Dev *56*, 1-7. 10.1016/j.gde.2019.04.006.
5. Nigg, E.A., and Raff, J.W. (2009). Centrioles, centrosomes, and cilia in health and disease. Cell *139*, 663-678. 10.1016/j.cell.2009.10.036.
6. Reiter, J.F., and Leroux, M.R. (2017). Genes and molecular pathways underpinning ciliopathies. Nat Rev Mol Cell Biol *18*, 533-547. 10.1038/nrm.2017.60.
7. Chen, X., Shi, Z., Yang, F., Zhou, T., and Xie, S. (2023). Deciphering cilia and ciliopathies using proteomic approaches. FEBS J *290*, 2590-2603. 10.1111/febs.16538.
8. Ostrowski, L.E., Blackburn, K., Radde, K.M., Moyer, M.B., Schlatzer, D.M., Moseley, A., and Boucher, R.C. (2002). A proteomic analysis of human cilia: identification of novel components. Mol Cell Proteomics *1*, 451-465. 10.1074/mcp.m200037-mcp200.
9. Blackburn, K., Bustamante-Marin, X., Yin, W., Goshe, M.B., and Ostrowski, L.E. (2017). Quantitative Proteomic Analysis of Human Airway Cilia Identifies Previously Uncharacterized Proteins of High Abundance. J Proteome Res *16*, 1579-1592. 10.1021/acs.jproteome.6b00972.
10. Sim, H.J., Yun, S., Kim, H.E., Kwon, K.Y., Kim, G.H., Kim, B.G., Myung, K., Park, T.J., and Kwon, T. (2020). Simple Method To Characterize the Ciliary Proteome of Multiciliated Cells. J Proteome Res *19*, 391-400. 10.1021/acs.jproteome.9b00589.
11. Boesger, J., Wagner, V., Weisheit, W., and Mittag, M. (2009). Analysis of flagellar phosphoproteins from Chlamydomonas reinhardtii. Eukaryot Cell *8*, 922-932. 10.1128/EC.00067-09.
12. Broadhead, R., Dawe, H.R., Farr, H., Griffiths, S., Hart, S.R., Portman, N., Shaw, M.K., Ginger, M.L., Gaskell, S.J., McKean, P.G., and Gull, K. (2006). Flagellar motility is required for the viability of the bloodstream trypanosome. Nature *440*, 224-227. 10.1038/nature04541.
13. Subota, I., Julkowska, D., Vincensini, L., Reeg, N., Buisson, J., Blisnick, T., Huet, D., Perrot, S., Santi-Rocca, J., Duchateau, M., et al. (2014). Proteomic analysis of intact flagella of procyclic Trypanosoma brucei cells identifies novel flagellar proteins with unique sub-localization and dynamics. Mol Cell Proteomics *13*, 1769-1786. 10.1074/mcp.M113.033357.
14. Pazour, G.J., Agrin, N., Leszyk, J., and Witman, G.B. (2005). Proteomic analysis of a eukaryotic cilium. J Cell Biol *170*, 103-113. 10.1083/jcb.200504008.
15. Lee, J., Møller, A.F., Chae, S., Bussek, A., Park, T.J., Kim, Y., Lee, H.S., Pers, T.H., Kwon, T., Sedzinski, J., and Natarajan, K.N. (2023). A single-cell, time-resolved profiling of. Sci Adv *9*, eadd5745. 10.1126/sciadv.add5745.
16. Walentek, P. (2021). Xenopus epidermal and endodermal epithelia as models for mucociliary epithelial evolution, disease, and metaplasia. Genesis *59*, e23406. 10.1002/dvg.23406.
17. Werner, M.E., and Mitchell, B.J. (2012). Understanding ciliated epithelia: the power of Xenopus. Genesis *50*, 176-185. 10.1002/dvg.20824.
18. Werner, M.E., and Mitchell, B.J. (2013). Using Xenopus skin to study cilia development and function. Methods Enzymol *525*, 191-217. 10.1016/B978-0-12-397944-5.00010-9.
19. Angerilli, A., Smialowski, P., and Rupp, R.A. (2018). The Xenopus animal cap transcriptome: building a mucociliary epithelium. Nucleic Acids Res *46*, 8772-8787. 10.1093/nar/gky771.
20. Elsayyid, M., Tanis, J.E., and Yu, Y. (2025). Simple In-Cell Processing Enables Deep Proteome Analysis of Low-Input. Anal Chem *97*, 9159-9167. 10.1021/acs.analchem.4c05003.

21. Martin, K.R., Le, H.T., Abdelgawad, A., Yang, C., Lu, G., Keffer, J.L., Zhang, X., Zhuang, Z., Asare-Okai, P.N., Chan, C.S., et al. (2024). Development of an efficient, effective, and economical technology for proteome analysis. Cell Rep Methods *4*, 100796. 10.1016/j.crmeth.2024.100796.
22. Stubbs, J.L., Vladar, E.K., Axelrod, J.D., and Kintner, C. (2012). Multicilin promotes centriole assembly and ciliogenesis during multiciliate cell differentiation. Nat Cell Biol *14*, 140-147. 10.1038/ncb2406.
23. Ma, L., Quigley, I., Omran, H., and Kintner, C. (2014). Multicilin drives centriole biogenesis via E2f proteins. Genes Dev *28*, 1461-1471. 10.1101/gad.243832.114.
24. Guo, T., Lu, C., Yang, D., Lei, C., Liu, Y., Xu, Y., Yang, B., Wang, R., and Luo, H. (2022). Case Report:. Front Genet *13*, 934920. 10.3389/fgene.2022.934920.
25. Kott, E., Legendre, M., Copin, B., Papon, J.F., Dastot-Le Moal, F., Montantin, G., Duquesnoy, P., Piterboth, W., Amram, D., Bassinet, L., et al. (2013). Loss-of-function mutations in RSPH1 cause primary ciliary dyskinesia with central-complex and radial-spoke defects. Am J Hum Genet *93*, 561-570. 10.1016/j.ajhg.2013.07.013.
26. Zariwala, M.A., Leigh, M.W., Ceppa, F., Kennedy, M.P., Noone, P.G., Carson, J.L., Hazucha, M.J., Lori, A., Horvath, J., Olbrich, H., et al. (2006). Mutations of DNAI1 in primary ciliary dyskinesia: evidence of founder effect in a common mutation. Am J Respir Crit Care Med *174*, 858-866. 10.1164/rccm.200603-370OC.
27. Spektor, A., Tsang, W.Y., Khoo, D., and Dynlacht, B.D. (2007). Cep97 and CP110 suppress a cilia assembly program. Cell *130*, 678-690. 10.1016/j.cell.2007.06.027.
28. Schmidt, K.N., Kuhns, S., Neuner, A., Hub, B., Zentgraf, H., and Pereira, G. (2012). Cep164 mediates vesicular docking to the mother centriole during early steps of ciliogenesis. J Cell Biol *199*, 1083-1101. 10.1083/jcb.201202126.
29. van Dam, T.J., Wheway, G., Slaats, G.G., Huynen, M.A., Giles, R.H., and Group, S.S. (2013). The SYSCILIA gold standard (SCGSv1) of known ciliary components and its applications within a systems biology consortium. Cilia *2*, 7. 10.1186/2046-2530-2-7.
30. Quigley, I.K., and Kintner, C. (2017). Rfx2 Stabilizes Foxj1 Binding at Chromatin Loops to Enable Multiciliated Cell Gene Expression. PLoS Genet *13*, e1006538. 10.1371/journal.pgen.1006538.
31. Choi, Y.J., Hwang, K.C., Park, J.Y., Park, K.K., Kim, J.H., Park, S.B., Hwang, S., Park, H., and Park, C. (2010). Identification and characterization of a novel mouse and human MOPT gene containing MORN-motif protein in testis. Theriogenology *73*, 273-281. 10.1016/j.theriogenology.2009.09.010.
32. Du, Y., and Wang, P. (2019). Upregulation of MIIP regulates human breast cancer proliferation, invasion and migration by mediated by IGFBP2. Pathol Res Pract *215*, 152440. 10.1016/j.prp.2019.152440.
33. Yu, X., Ng, C.P., Habacher, H., and Roy, S. (2008). Foxj1 transcription factors are master regulators of the motile ciliogenic program. Nat Genet *40*, 1445-1453. 10.1038/ng.263.
34. Antoniades, I., Stylianou, P., and Skourides, P.A. (2014). Making the connection: ciliary adhesion complexes anchor basal bodies to the actin cytoskeleton. Dev Cell *28*, 70-80. 10.1016/j.devcel.2013.12.003.
35. Kulkarni, S.S., Griffin, J.N., Date, P.P., Liem, K.F., and Khokha, M.K. (2018). WDR5 Stabilizes Actin Architecture to Promote Multiciliated Cell Formation. Dev Cell *46*, 595-610.e593. 10.1016/j.devcel.2018.08.009.
36. Sedzinski, J., Hannezo, E., Tu, F., Biro, M., and Wallingford, J.B. (2016). Emergence of an Apical Epithelial Cell Surface In Vivo. Dev Cell *36*, 24-35. 10.1016/j.devcel.2015.12.013.
37. Zhao, H., Sun, J., Insinna, C., Lu, Q., Wang, Z., Nagashima, K., Stauffer, J., Andresson, T., Specht, S., Perera, S., et al. (2022). Male infertility-associated Ccdc108 regulates multiciliogenesis via the intraflagellar transport machinery. EMBO Rep *23*, e52775. 10.15252/embr.202152775.
38. Lee, M., Nagashima, K., Yoon, J., Sun, J., Wang, Z., Carpenter, C., Lee, H.K., Hwang, Y.S., Westlake, C.J., and Daar, I.O. (2022). CEP97 phosphorylation by Dyrk1a is critical for centriole separation during multiciliogenesis. J Cell Biol *221*. 10.1083/jcb.202102110.
39. Lee, M., Hwang, Y.S., Yoon, J., Sun, J., Harned, A., Nagashima, K., and Daar, I.O. (2019). Developmentally regulated GTP-binding protein 1 modulates ciliogenesis via an interaction with Dishevelled. J Cell Biol *218*, 2659-2676. 10.1083/jcb.201811147.

40. Benmerah, A. (2013). The ciliary pocket. Curr Opin Cell Biol *25*, 78-84. 10.1016/j.ceb.2012.10.011.
41. Son, J.H., Park, J.S., Lee, J.U., Kim, M.K., Min, S.A., Park, C.S., and Chang, H.S. (2022). A genome-wide association study on frequent exacerbation of asthma depending on smoking status. Respir Med *199*, 106877. 10.1016/j.rmed.2022.106877.
42. Zein, J., Owora, A., Kim, H.J., Marozkina, N., and Gaston, B. (2024). Asthma Among Children With Primary Ciliary Dyskinesia. JAMA Netw Open *7*, e2449795. 10.1001/jamanetworkopen.2024.49795.
43. Moody, S.A. (2000). Cell lineage analysis in Xenopus embryos. Methods Mol Biol *135*, 331-347. 10.1385/1-59259-685-1:331.
44. Bruderer, R., Bernhardt, O.M., Gandhi, T., Miladinović, S.M., Cheng, L.Y., Messner, S., Ehrenberger, T., Zanotelli, V., Butscheid, Y., Escher, C., et al. (2015). Extending the limits of quantitative proteome profiling with data-independent acquisition and application to acetaminophen-treated three-dimensional liver microtissues. Mol Cell Proteomics *14*, 1400-1410. 10.1074/mcp.M114.044305.

XPERIMENTAL MODEL AND STUDY PARTICIPANT DETAILS

Xenopus laevis and Xenopus tropicalis

Wild-type *Xenopus laevis* and *Xenopus tropicalis* were purchased from National *Xenopus* Resource in Woods Hole, Massachusetts. Methods involving live animals were carried out in accordance with the guidelines and regulations approved and enforced by the Institutional Animal Care and Use Committees at University of Delaware.

METHOD DETAILS

Plasmids

Coding sequences of *Xenopus tropicalis* Ccdc30, Morn2, Wdr88, Miip was cloned by PCR from stage 18 and stage 25 embryo cDNA and subcloned into pCS2^{+}-HA and pCS2^{+}-GFP vectors.

***Xenopus* embryo, morpholinos and microinjection**

Xenopus embryos were obtained by standard methods.[43] Capped sense RNAs were transcribed using the mMessage mMachine SP6 kit (ThermoFisher). Embryos were injected with mRNAs or morpholinos one-cell or four-cell stage. The following mRNAs were used: memGFP (100 pg); *Morn2-HA* (250 pg); *Ccdc30-HA* (300 pg); *Wdr88-GFP* (200 pg); *Morn2-GFP* (200 pg); *Ccdc30-GFP* (250 pg); *Miip-GFP* (200 pg); *Centrin4-RFP* (50 pg); *MCI-GR* (40 pg). Protein activity of GR chimeric constructs was induced by incubating the embryos in 4 µg/ml dexamethasone from stage 11–26. The morpholinos were obtained from Gene Tools. 7 ng Con MO or Morn2 MO or Ccdc30 MO was injected per *Xenopus tropicalis* embryo.

Whole-mount *in situ* hybridization

Digoxigenin-labeled antisense RNA probes were synthesized using T3 polymerase. Whole-mount *in situ* hybridization were performed by standard methods using probes for *Ccdc30, Wdr88, Morn2 and Miip in Xenopus tropicalis embryos.*

Antibodies

Primary antibodies used included: mouse anti-acetylated tubulin-594 (1:1000, Proteintech), Rat anti-HA (1:500, Sigma) and rabbit anti-CEP164 (1:400, Proteintech). Secondary antibodies conjugated to Alexa Fluor dyes were used at 1:1000.

Immunofluorescence microscopy

Embryos were fixed with 4% formaldehyde at 4°C overnight and then dehydrated with 100% methanol. The following primary antibodies were used: Primary antibodies used included: mouse anti-acetylated tubulin-594 (1:1000, Proteintech), Rat anti-HA (1:500, Sigma) and rabbit anti-CEP164 (1:400, Proteintech). Secondary antibodies conjugated to Alexa Fluor dyes were used at 1:1000. The samples were mounted in ProLong Gold and imaged using dragonfly spinning disk confocal microscope or Zeiss LSM880 laser scanning confocal microscope.

Live imaging

For live imaging, embryos expressing GFP-tagged constructs were mounted in 0.1× MMR with. Z-stacks imaging was acquired on dragonfly spinning disk confocal microscope.

Electron Microscopy

The embryos were fixed in 2% paraformaldehyde, 2% glutaraldehyde in 0.1M sodium cacodylate buffer, rinsed in buffer then fixed in 1% osmium tetroxide in 0.1M sodium cacodylate buffer. They were dehydrated in ascending concentrations of ethanol (25% to 100%) then hexamethyldisilazane and air dried. The dried samples were mounted on SEM stubs and sputter coated with platinum in a Leica EM ACE600 coater (Vienna, Austria). SEM images were acquired using a ThermoFisher Scientific Apreo Volumescope SEM (Hillsboro, OR).

Embryo gliding assay

Stage 27 embryos were placed in 0.1× MMR on agar-coated dishes. Time-lapse videos were captured using a Zeiss stereo microscope. Movement trajectories were quantified using imageJ's Manual tracking plugin.

Protein sample preparation and LC-MS/ analysis

For in-cell sample preparation, eight stage26 *Xenopus laevis* animal caps (Dex+ or Dex-) were collected and transferred to E4tips XL (CDS Analytical, Oxford, PA) that were prefilled with 200 µl of methanol, and incubated on ice for 30 minutes. Three replicates were prepared. The tips containing fixed embryos were processed following a protocol described previously.[20] Briefly, the tips were first spun at 1,500 x g for one minute and washed one time with 200 µl of methanol. Then 100 µl of 50 mM triethylammonium bicarbonate (TEAB) with final concentration of 10 mM Tris (2-carboxyethyl) phosphine (TCEP) and 40 mM chloroacetamide (CAA) was added, followed by incubation at 45□C for 10-15 min. The E4tips were then washed one time with 200 µl 50 mM TEAB. For protein digestion, 150 µl 50 mM TEAB plus 1.0 µg of trypsin/Lys-C mix (Promega, WI) was added to the samples and incubated at 37□C for 16-18 hours with gentle shaking (350 rpm/min). After digestion, the samples were acidified with 1% formic acid (final concentration) and spun at low speed (400-600 x g) for 10 min. The tips were washed one time with 200 µl of wash buffer (0.5% acetic acid in water) to discard flow through. The tips were transferred to new collection tubes, and subjected to two sequential elution with 200 µl of Elution buffer I (60% acetonitrile and 0.5% acetic acid in water) and Elution buffer II (80% ACN and 0.5% acetic acid in water), respectively. The elution was pooled, dried in the SpeedVac, and then stored at -80□C until further analysis.

LC-MS/MS analysis

The LC-MS/MS analysis was conducted with an Ultimate 3000 RSLCnano system coupled to an Orbitrap Eclipse mass spectrometer and FAIMS Pro Interface (Thermo Scientific). The peptides were resuspended in 15 µl of LC buffer A (0.1% formic acid in water), and 10 µl of it was loaded onto a trap column (PepMap100 C18, 300 µm × 2 mm, 5 µm; Thermo Scientific) followed by separation on an analytical column (PepMap100 C18, 50 cm × 75 µm i.d., 3 µm; Thermo Scientific) flowing at 250 nL/min. A linear LC gradient was applied from 1% to 25% mobile phase B over 125 min, followed by an increase to 32% mobile phase B over 10 min. The column was washed with 80% mobile phase B for 5 min, followed by equilibration with mobile phase A for 15 min. For the ion source settings, the spray voltage was set to 1.9 kV, funnel RF level at 50%, and heated capillary temperature at 275°C. The MS data were acquired in Orbitrap at 120K resolution, followed by MS/MS acquisition in data-independent mode following a protocol described previously.[21] For FAIMS analysis, a 3-CV experiment (−40|-55|-75) was applied. The MS scan range (m/z) was set to 380-985, maximum injection time was 246ms, and normalized AGC target was 100%. For MS/MS acquisition, the isolation mode was Quadrupole, isolation window was 8 m/z, and window overlap was 1 m/z. The collision energy was 30%, Orbitrap resolution was 30K, AGC Target was 400K, and normalized AGC target was 800%.

Proteome quantitation and data analysis

Mass spec data were processed using Spectronaut software (version 19.5)[44] and a library-free DIA analysis workflow with directDIA+ and the *X. laevis* protein database (UniProt 2025 release; 111,661 sequences). Briefly, the settings for Pulsar and library generation include: Trypsin/P as specific enzyme; peptide length from 7 to 52 amino acids; allowing 2 missed cleavages; toggle N-terminal M turned on; Carbamidomethyl on C as fixed modification; Oxidation on M and Acetyl at protein N-terminus as variable modifications; FDRs at PSM, peptide and protein level all set to 0.01; Quantity MS level set to MS2, and cross-run normalization turned on. Bioinformatics analyses including t-test, correlation, volcano plot and clustering analyses were performed using Perseus software (version 1.6.2.3) and Prism GraphPad (version 10) unless otherwise indicated.

Statistical Analysis

Statistical significance was assessed using unpaired two-tailed Student's t-tests for comparisons between two groups. p-values < 0.05 were considered statistically significant. All statistical analyses were performed using GraphPad Prism10.

A

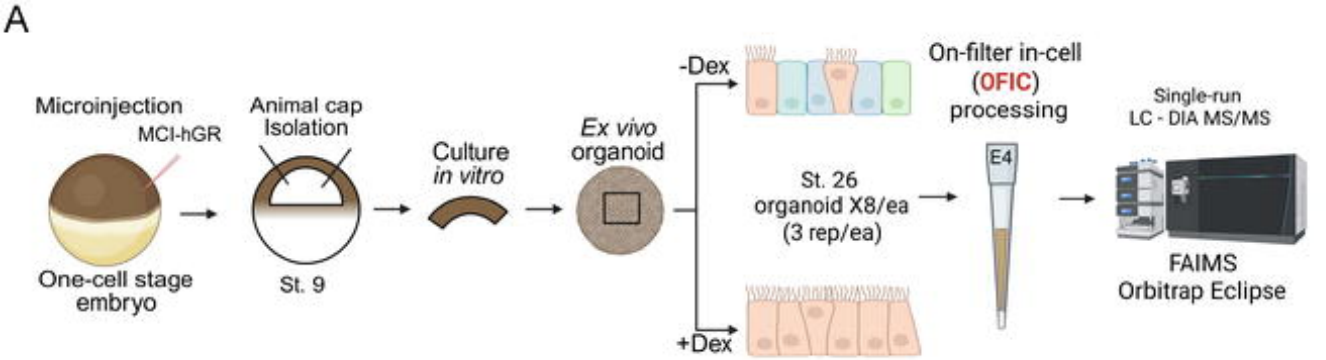
Microinjection
MCI-hGR
One-cell stage embryo
Animal cap Isolation
St. 9
Culture in vitro
Ex vivo organoid
-Dex
+Dex
St. 26 organoid X8/ea (3 rep/ea)
On-filter in-cell (OFIC) processing
E4
Single-run LC - DIA MS/MS
FAIMS Orbitrap Eclipse

B

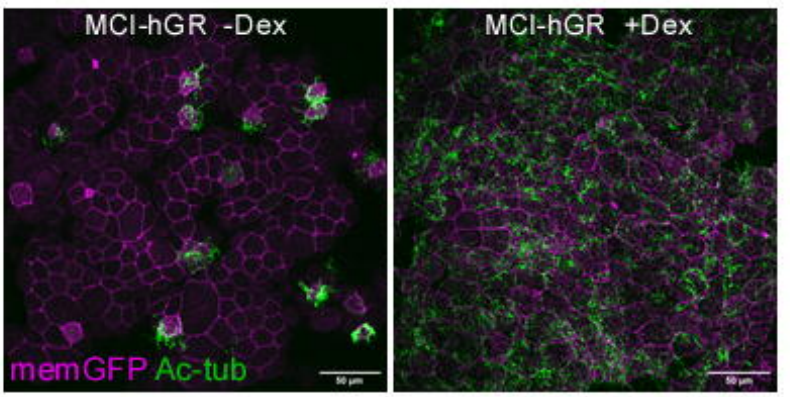
MCI-hGR -Dex
MCI-hGR +Dex
memGFP Ac-tub

C

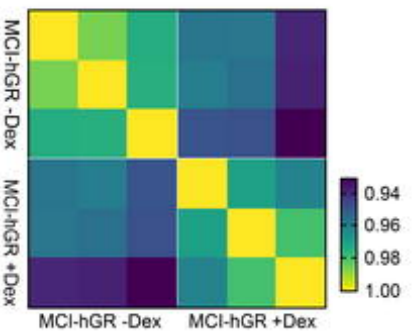
MCI-hGR -Dex
MCI-hGR +Dex
0.94
0.96
0.98
1.00

D

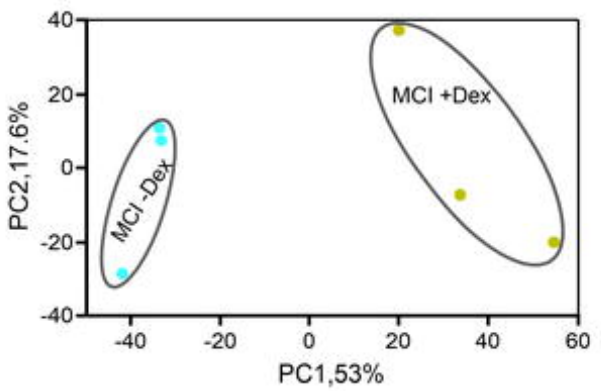
MCI -Dex
MCI +Dex
PC2,17.6%
PC1,53%

E

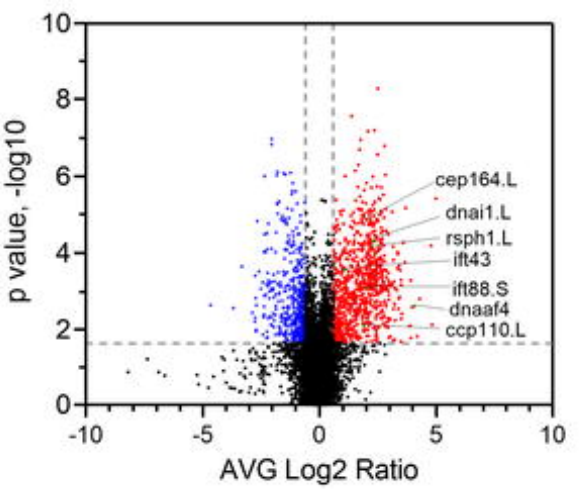
p value, -log10
AVG Log2 Ratio
cep164.L
dnai1.L
rsph1.L
ift43
ift88.S
dnaaf4
ccp110.L

F

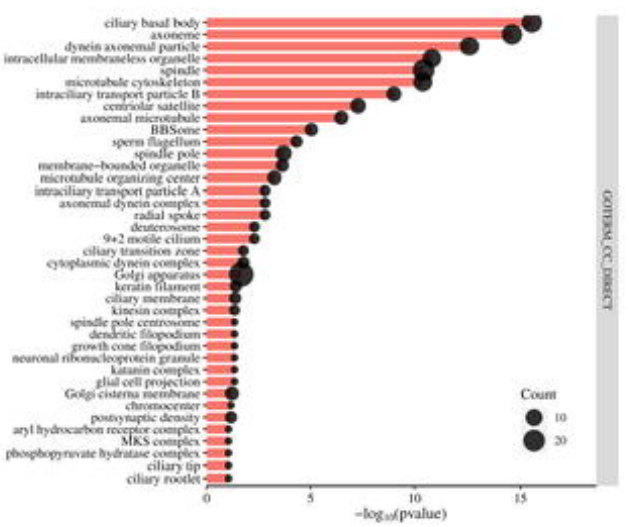
ciliary basal body
axoneme
dynein axonemal particle
intracellular membraneless organelle
spindle
microtubule cytoskeleton
intraciliary transport particle B
centriolar satellite
axonemal microtubule
BBSome
sperm flagellum
spindle pole
membrane-bounded organelle
microtubule organizing center
intraciliary transport particle A
axonemal dynein complex
radial spoke
deuterosome
9+2 motile cilium
ciliary transition zone
cytoplasmic dynein complex
Golgi apparatus
keratin filament
ciliary membrane
kinesin complex
spindle pole centrosome
dendritic filopodium
growth cone filopodium
neuronal ribonucleoprotein granule
katanin complex
glial cell projection
Golgi cisterna membrane
chromocenter
postsynaptic density
aryl hydrocarbon receptor complex
MKS complex
phosphopyruvate hydratase complex
ciliary tip
ciliary rootlet
Count
10
20
0
5
10
15
−log10(pvalue)

G

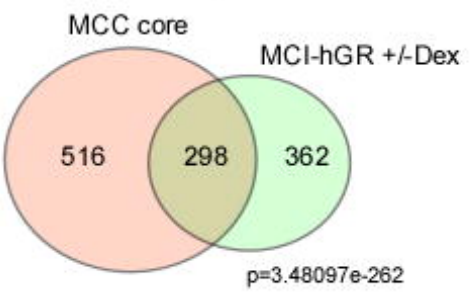
MCC core
MCI-hGR +/-Dex
516
298
362
p=3.48097e-262

H

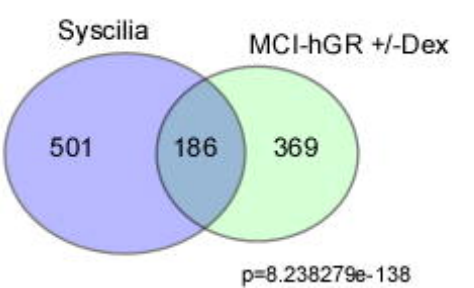
Syscilia
MCI-hGR +/-Dex
501
186
369
p=8.238279e-138

A

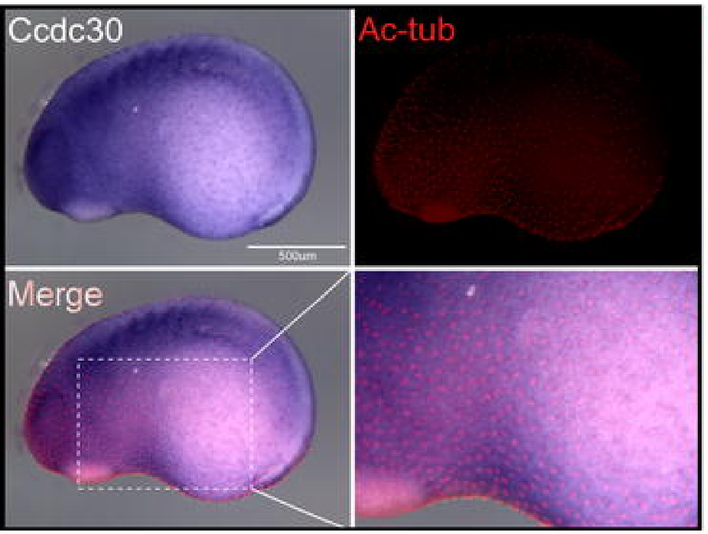
Ccdc30
Ac-tub
Merge

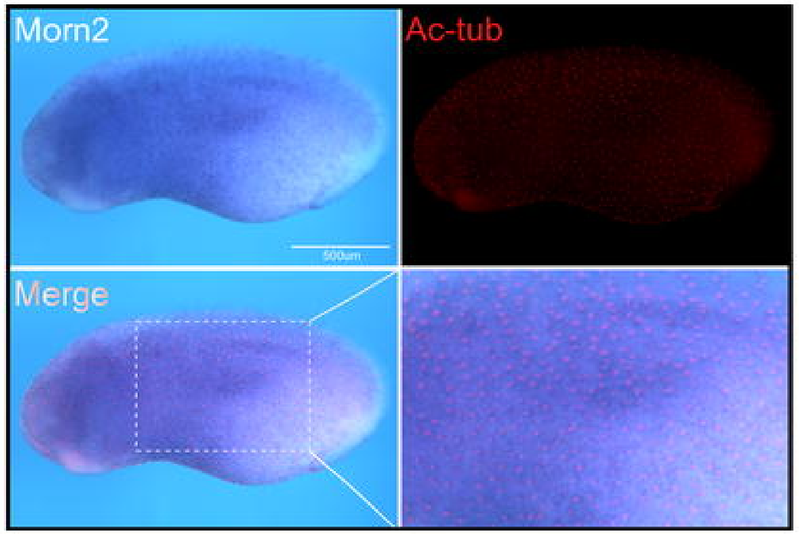
Morn2
Ac-tub
Merge

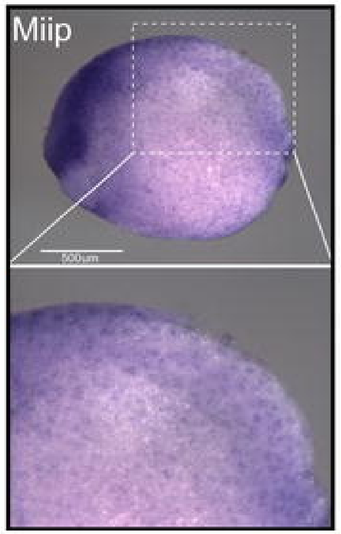
Miip

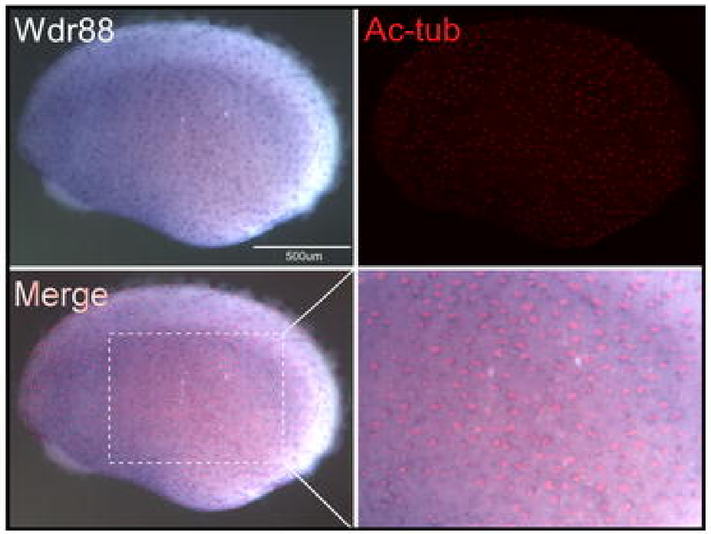
Wdr88
Ac-tub
Merge

B

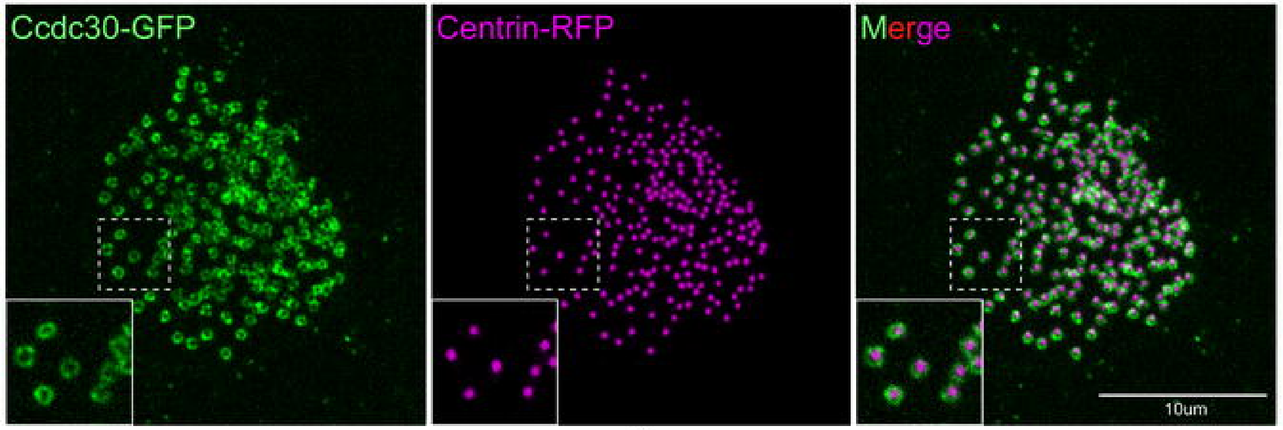
Ccdc30-GFP
Centrin-RFP
Merge
10um

C

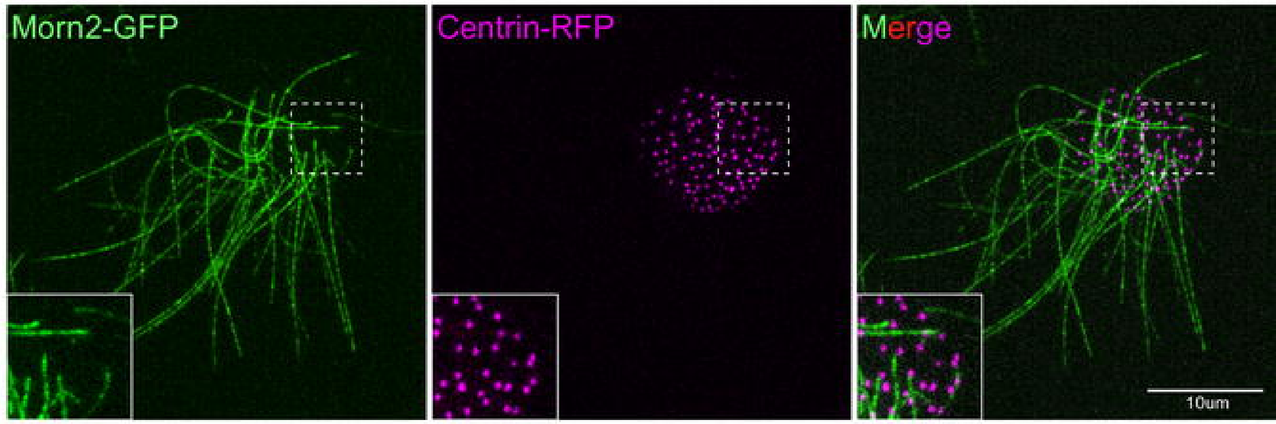
Morn2-GFP
Centrin-RFP
Merge
10um

D

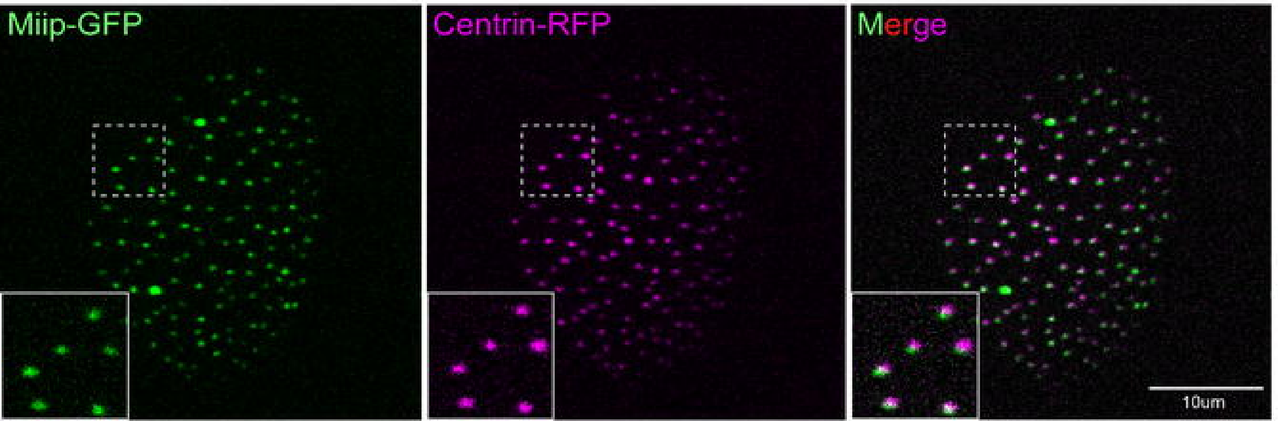
Miip-GFP
Centrin-RFP
Merge
10um

E

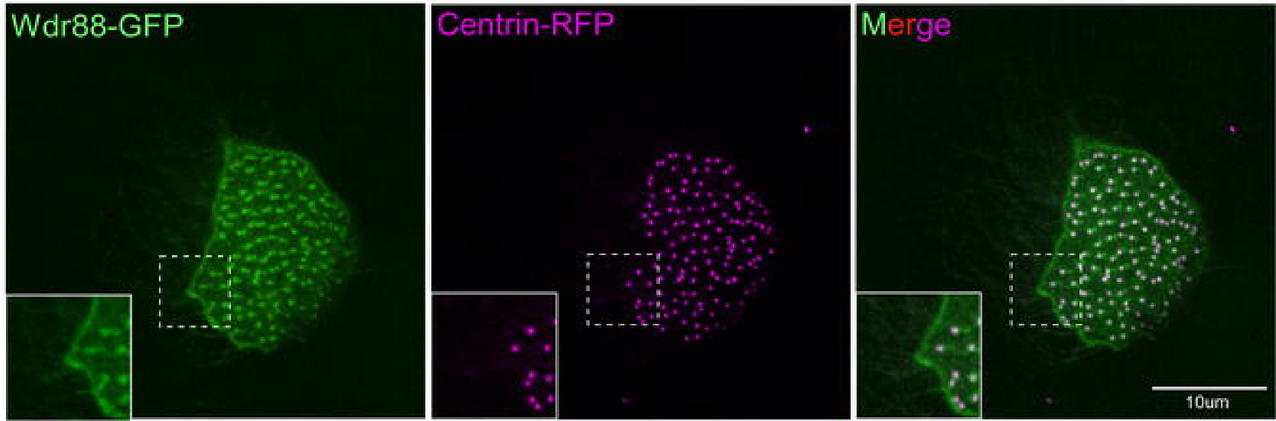
Wdr88-GFP
Centrin-RFP
Merge
10um

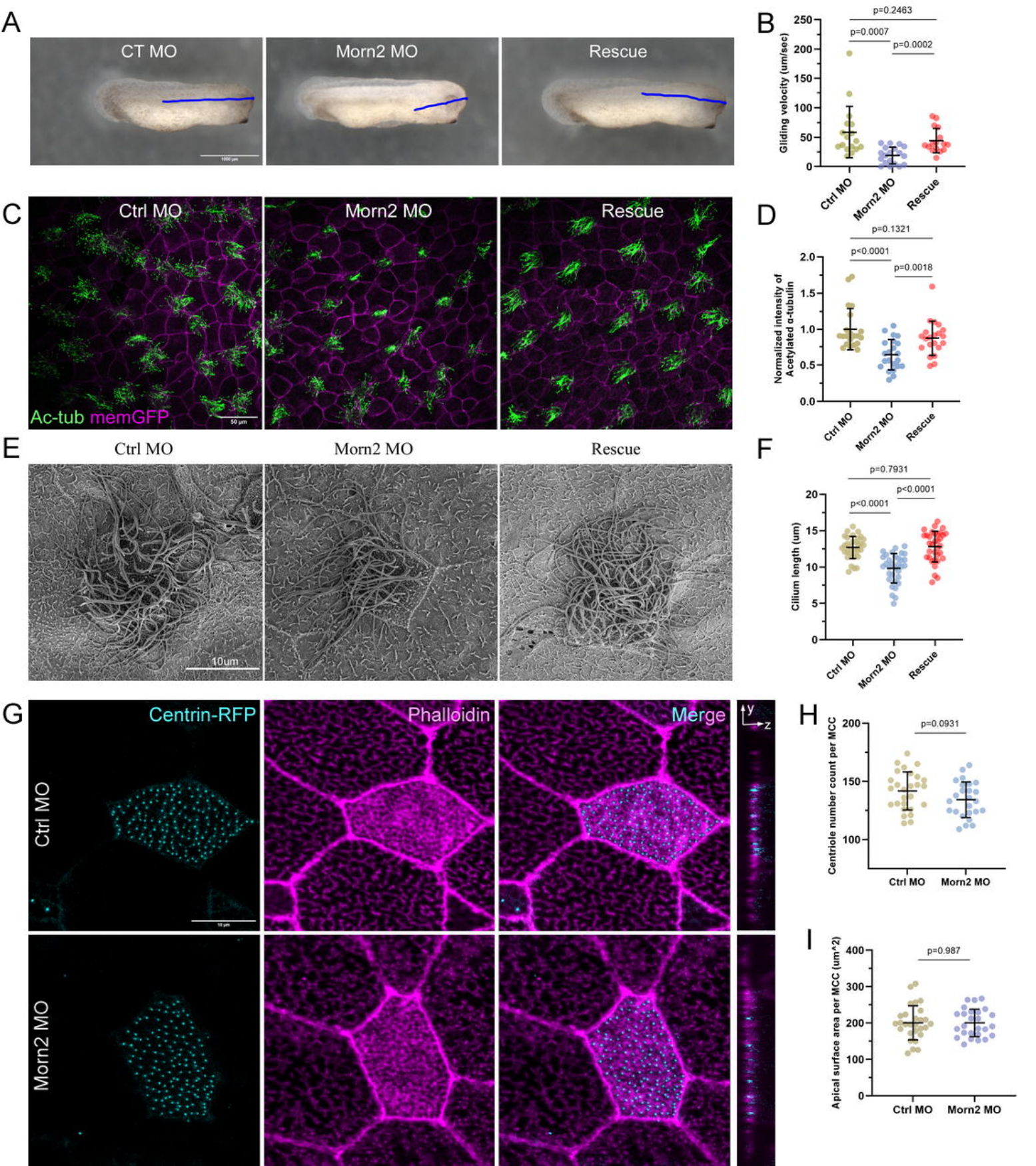
A
CT MO
Morn2 MO
Rescue
B
p=0.2463
p=0.0007
p=0.0002
Gliding velocity (um/sec)
250
200
150
100
50
0
Ctrl MO
Morn2 MO
Rescue
C
Ctrl MO
Morn2 MO
Rescue
Ac-tub memGFP
50 µm
D
p=0.1321
p<0.0001
p=0.0018
Normalized intensity of Acetylated α-tubulin
2.0
1.5
1.0
0.5
0.0
Ctrl MO
Morn2 MO
Rescue
E
Ctrl MO
Morn2 MO
Rescue
10um
F
p=0.7931
p<0.0001
p<0.0001
Cilium length (um)
20
15
10
5
0
Ctrl MO
Morn2 MO
Rescue
G
Centrin-RFP
Phalloidin
Merge
y
z
Ctrl MO
Morn2 MO
H
p=0.0931
Centriole number count per MCC
200
150
100
Ctrl MO
Morn2 MO
I
p=0.987
Apical surface area per MCC (um^2)
400
300
200
100
0
Ctrl MO
Morn2 MO

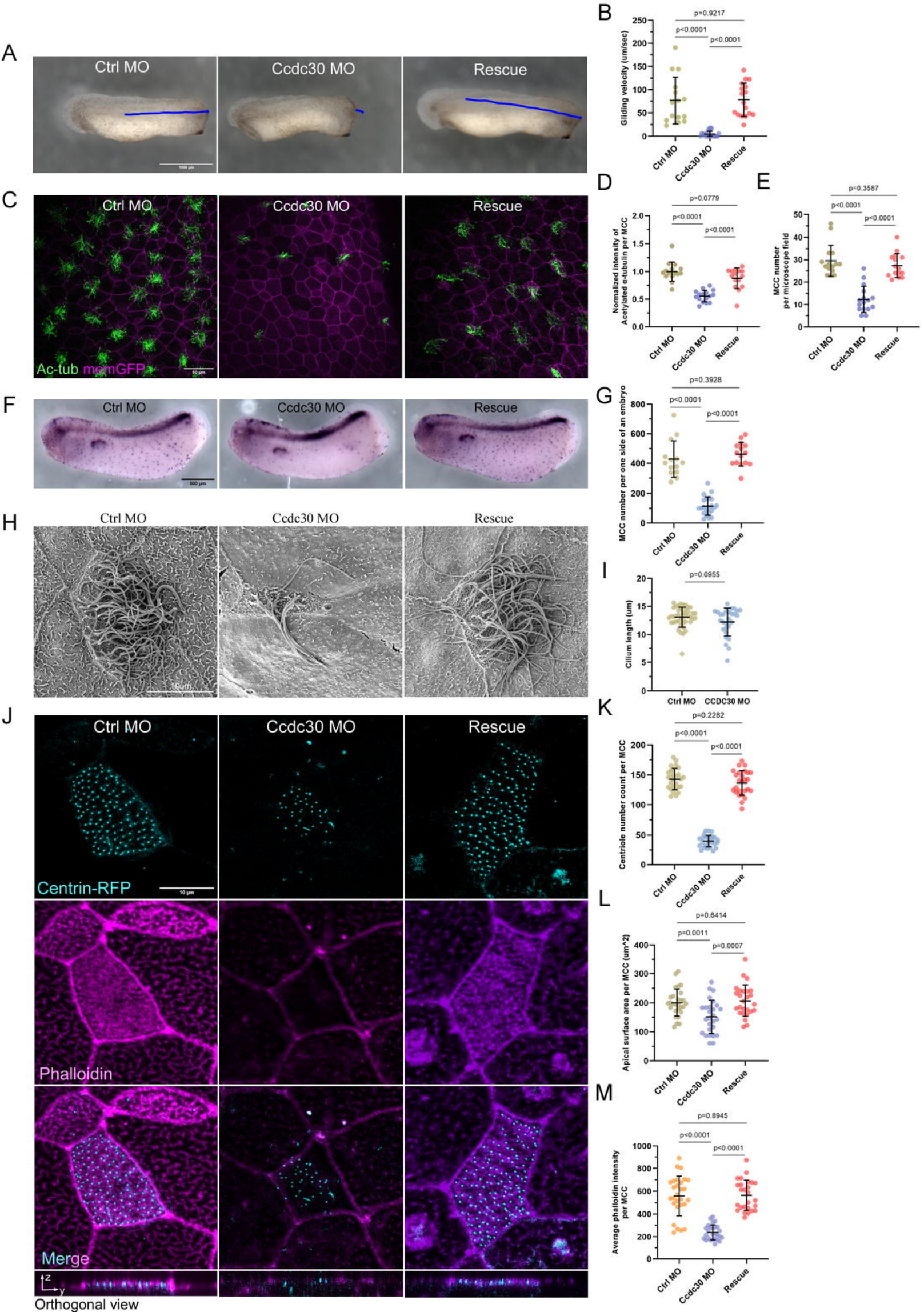
A
Ctrl MO
Ccdc30 MO
Rescue
B
Gliding velocity (um/sec)
p=0.9217
p<0.0001
p<0.0001
C
Ac-tub mem-GFP
D
Normalized intensity of Acetylated α-tubulin per MCC
p=0.0779
p<0.0001
p<0.0001
E
MCC number per microscope field
p=0.3587
p<0.0001
p<0.0001
F
G
MCC number per one side of an embryo
p=0.3928
p<0.0001
p<0.0001
H
I
Cilium length (um)
p=0.0955
CCDC30 MO
J
Centrin-RFP
Phalloidin
Merge
Orthogonal view
K
Centriole number count per MCC
p=0.2282
p<0.0001
p<0.0001
L
Apical surface area per MCC (um^2)
p=0.6414
p=0.0011
p=0.0007
M
Average phalloidin intensity per MCC
p=0.8945
p<0.0001
p<0.0001